

Effects of non-isothermal aging on microstructure, mechanical properties and corrosion behaviors of a high Zn-containing Al-Zn-Mg-Cu-Zr alloy

Longlong He, Lanping Huang, Shumin Fan, Kanghua Chen

Science and Technology on High Strength Structural Materials Laboratory, Central South University, Changsha 410083, China

E-mail address: christie@csu.edu.cn

Abstract—The microstructure, mechanical properties and corrosion behaviors of an ultrahigh strength Al-Zn-Mg-Cu-Zr alloy subjected to the non-isothermal aging process have been investigated. When target aging temperature is between 180 °C and 190 °C during non-isothermal aging, the hardness of 7056 Al alloy reaches the maximum of 210 HV and its tensile strength is more than 700 MPa. With target aging temperature further increases to 200 °C, the hardness of the alloy rapidly decreases due to the coarsening of the precipitates in grain interiors. With the increase of target aging temperature and aging time, the resistance to intergranular corrosion (IGC) and exfoliation corrosion (EXCO) can also be enhanced due to the gradually coarsening and disconnecting of grain boundary precipitates.

Keywords—Al-Zn-Mg-Cu alloy; non-isothermal aging; microstructure; mechanical properties; corrosion resistance

I. INTRODUCTION

Al-Zn-Mg-Cu alloys (7xxx series) have been extensively used as structural materials in aerospace and automotive industry due to their excellent properties, such as low density, high strength, good workability and corrosion resistance [1-3]. However, to further satisfy the increasing demands for the comprehensive properties of high-strength aluminum alloys in the future, various methods have been developed, focusing on alloy composition optimization, manufacturing process, severe deformation and heat treatment [4-12]. Among these, heat treatment, especially aging process, has been an effective and critical way to control the microstructure and properties of Al-Zn-Mg-Cu alloys since the precipitates formed during aging act as the key strengthening mechanism and heavily determine mechanical properties and corrosion features of the alloys.

It is well known that aging tempers mainly affect geometrical characteristics of the precipitates and their mismatch relationship with Al alloy matrix and thus bring forth different performances to the alloys. These aging processes can be categorized as isothermal aging involving one or a series of isothermal procedures, which is usually convenient to be carried out precisely in most applications. However, the

accuracy and controllability of isothermal aging have been obviously limited when being performed on large components due to the temperature-lagging effect in them during the heating and/or cooling stage. Therefore, the non-isothermal aging process has been developed to accommodate heating and/or cooling procedures for the purpose of further enhancing mechanical properties of Al alloys. The feasibility of the non-isothermal aging in Al-Zn-Mg-Cu alloys has been widely examined. For example, James et.al have proposed an improved non-isothermal aging for Al-Zn-Mg-Cu alloys and investigated the effects of heating rate on the properties [13]. Jiang et.al also found that the heating aging enhances mechanical properties and retains corrosion resistance of Al-Zn-Mg-Cu alloy comparable to that of over-aging condition [14]. The researchers have mainly focused the precipitation behaviors and the resulted performance evolving in non-isothermal aging for Al-Zn-Mg-Cu alloys, and the zinc content of these investigated alloys is not high, no more than 9 wt.% [14-19]. In fact, the Al-Zn-Mg-Cu alloys containing high Zn more than 9 wt.% exhibit higher strength and improved overall performance suitable for aerospace applications. However, the work on non-isothermal aging of high-Zn containing Al-Zn-Mg-Cu alloys is rarely reported. In this work, the influences of the ending aging temperature and heating rate on the microstructure, mechanical and corrosion properties of 7056 Al alloy with Zn more than 9 wt.% during non-isothermal aging have been investigated and discussed in detail.

II. EXPERIMENTAL PROCEDURES

The nominal chemical composition of 7056 aluminum alloy is listed in Table 1. The alloy ingots were prepared by melting high-purity Al (99.99 wt.%), Mg (99.9 wt.%), Cu (99.9 wt.%), Zn (99.9 wt.%) as well as Al-5.1Zr and Al-4.95Ti master alloys in a resistance furnace. The melting temperature was kept at 700-750 °C, stirred vigorously and then cast into a graphite mold with the diameter of 110 mm. The cast ingots were homogenized step-by-step at 410 °C for 8 h, 465 °C for 6 h and subsequently 470 °C for 36 h, and then hot extruded into 12 mm thick plates at 450-460 °C with the extrusion ratio 9:1. The extruded plates were solution treated at 470 °C for 2 h and rapidly quenched into cold water (water temperature lower than 25 °C). During the subsequent non-isothermal aging process, the

specimens were heated from 60 °C to 210 °C at heating rates of 20, 40 and 60 °C/h, respectively. When heated to the target temperature, the specimens were taken out and quickly quenched into cold water. Finally, all the specimens were aged at 120 °C for 24 h.

The hardness measurements were carried out using Shanghai HV-50 Rockwell hardness tester. Tensile properties were performed on smooth plate specimens by an Instron 3369 testing machine at room temperature with a tensile speed of 2 mm/min. The gauge length and width of the specimen were 25 mm and 6 mm, respectively. Electrical conductivity was tested by an eddy current conductivity meter at room temperature. A JSM-6360LV scanning electron microscope (SEM) attached with energy dispersive spectroscopy (EDS) was applied for observing the morphology and distribution of second phase in Al alloy matrix and obtaining its compositional information. Microstructure was investigated by a JEM-2000FX transmission electron microscopy (TEM) with an operating voltage of 200 kV. Thin foils for TEM were prepared by mechanical polishing to 70 μm and final twin-jet electro-polishing in solution including 25% HNO₃ and 75% CH₃OH at -25 °C.

The intergranular corrosion (IGC) test was performed according to GB/T 7998-2005 standard [30], and the average intergranular corrosion depths were determined by optical microscopy (OM). The EXCO test was carried out according to GB/T 22639-2008 standard. The samples were immersed in the solution containing 4.0 M NaCl, 0.5 M KNO₃ and 0.1 M HNO₃, and visually inspected at regular intervals. The testing temperature was kept at 25±1 °C in a thermostat and the ratio of solution volume to metal surface was 20 mL/cm². The susceptibility of EXCO was assessed by reference to standard photographs N (No obvious attack), P (pitting), EA (superficial exfoliation), EB (moderate exfoliation), EC (severe exfoliation), and ED (very severe exfoliation).

Table 1 Nominal chemical composition of 7056 Al alloy (wt.%)

Alloy	Zn	Mg	Cu	Zr	Ti	Al
7056 alloy	9.1	1.8	1.6	0.13	0.01	Bal.

III. RESULTS AND DISCUSSION

The mechanical properties and corrosion resistance of Al alloy can be simply evaluated by measuring its hardness and electrical conductivity, respectively. The dependences of the hardness and electrical conductivity of 7056 Al alloys on the ending aging temperature at heating rates of 20, 40 and 60 °C/h are shown in Fig. 1. As a whole, it can be found from Fig. 1(a) that the variation tendency of the hardness for various heating rates is very similar. The hardness of the investigated alloy first tardily increases and then remains steady as the ending temperature rises, and finally decreases quickly. The increase of heating rate from 20 to 60 °C/h leads to an increase of the peak value of the hardness. The higher heating

rate, presents a lower hardness value at the same ending temperature. The peak hardness values of 7056 Al alloy for various heating rates all can be reached at the temperature range from 170 to 190 °C.

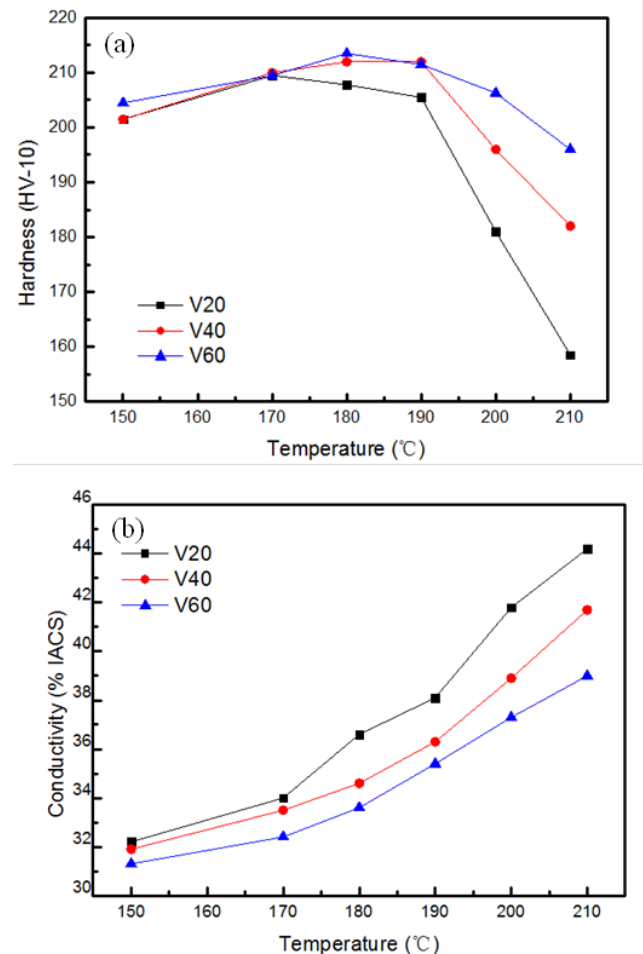


Figure 1 Effects of heating rate on (a) hardness and (b) electrical conductivity of 7056 Al alloys.

As for the electrical conductivity, as show in Fig. 1(b), the increase of heating rate from 20 to 60 °C/h results in a decrease in electrical conductivity with respect to various temperatures of terminated aging during non-isothermal aging. Besides, the electrical conductivity straightly increases with the increase of the ending aging temperature, and the increment becomes more obvious at higher temperature, which shows that the ending aging temperature and heating rate have obvious influence on the electrical conductivity of 7056 Al alloy. It is well known that the variation of electrical conductivity can indirectly reflect the decomposition of the supersaturation solid solution in alloys and be used for assessing the SCC resistance [20]. In Al-Zn-Mg-Cu alloys, the SCC resistance has been found to increase with the increase of electrical conductivity. The electrical conductivity usually increases greatly as a result of the reduction of electron scattering resulting from the decrease of solid solubility of supersaturation solid solution and the coarsening of precipitates during aging. When the heating rate is relatively high, the strengthening phase is difficult to grow up after nucleation due to short aging time. While the

strengthening phase obviously coarsens at low heating rate due to the distinct decrease of the supersaturation solid solubility. Therefore, the variation of electrical conductivity is obviously larger at the higher heating rate.

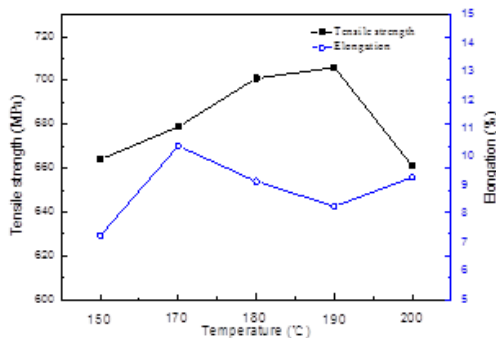


Figure 2 Variation of the ultimate tensile strength and elongation of 7056 Al alloy subjected to non-isothermal aging at a heating rate of 40 °C/h.

Figure 2 presents the variation of the ultimate tensile strength and elongation of the non-isothermal aged 7056 Al alloys with the ending aging temperature at a heating rate of 40°C/h. It can be found that the variation of tensile strength is very similar to the trend of micro-hardness variety shown in Fig.1 (a). The tensile strength steadily increases at the temperature range from 150 to 190 °C and is up to the peak strength of 706 MPa, and then rapidly decreases to 664 MPa when the ending temperature further rises to 200°C. The elongation of 7056 Al alloy is only 7.26 % when the ending temperature is 150 °C, and increases to 10.4 % when the temperature is 170°C. Hereafter, the elongation gradually decreases at the temperature range from 170 to 190°C. Continuous increasing temperature to 200 °C, the elongation increases again due to the over-aged state of the alloy.

Figure 3 shows the cross-section corrosion morphologies and maximum corrosion depths of the non-isothermal aged 7056 Al alloys at a heating rate of 40 °C/h. The corrosion depths are obviously influenced by the ending aging temperature during non-isothermal aging. The corrosion cracks propagate along grain boundaries into the interior under the surface of Al alloys. The damage corrosion extent can be assessed according to the maximum corrosion depth and global corrosion condition. When the ending aging temperature is 150 °C, the alloy is the most susceptible to the corrosion attack and the maximum corrosion depth extends up to 282 μm, as shown in Fig. 3(a). With increasing the ending aging temperature from 170 to 190 °C, the maximum corrosion depth slowly decreases from 275 to 241 μm due to the extension of aging time (shown in Fig. 3(b)-(d)). As to the ending aging temperature is over 190 °C, the maximum corrosion depth is 168 and 139 μm in Fig. 3(e) and (f), respectively. This means that the corrosion resistance of the 7056 Al alloys can be obviously enhanced by

increasing the ending aging temperature during non-isothermal aging.

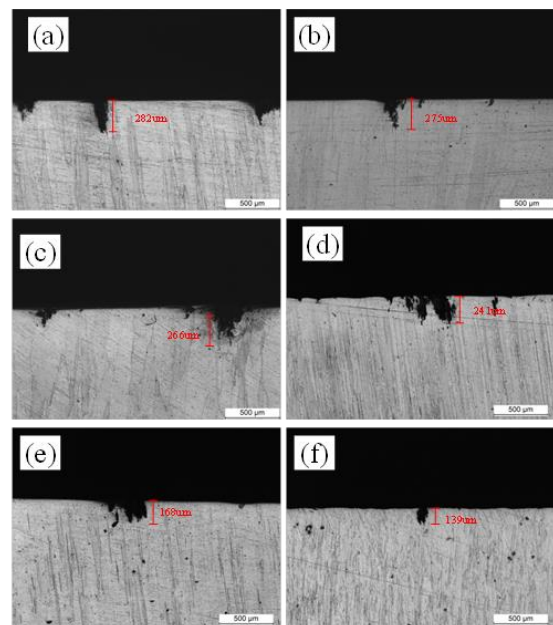


Figure 3 Cross-section corrosion morphologies and maximum corrosion depths of 7056 Al alloys aged at various ending aging temperatures at a heating rate of 40 °C/h: (a) 150 °C; (b) 170 °C; (c) 180 °C; (d) 190 °C; (e) 200 °C; (f) 210 °C.

The visual EXCO ratings of the non-isothermal aged 7056 Al alloys after immersion for various time are listed in Table 2. With the extension of immersion time, the degree of corrosion increases. It is clear that a corrosion rating of EA is given to the specimen with the ending aging temperature of 150 °C after immersion for 6 h, while the pitting associated with the preferential dissolution of active precipitates was the only attack for other specimens. When immersion for 6-48h, it can be found that the increase of the ending aging temperature enhances the EXCO corrosion resistance to some extent. When the ending aging temperature is not lower than 190 °C, the corrosion rate of EA can be kept after immersion for 48 h. However, other specimens are ranked as EB and EC.

Table 2 Visual EXCO ratings of the non-isothermal aged 7056 Al alloys after immersion for various time

Ending aging temperature	6h	12 h	24 h	48h
150 °C	EA	EB	EB +	EC
170 °C	PC	EA	EB	EC
180 °C	PB	EA	EA	EB
190 °C	PB	EC	EA	EA
200 °C	PA	PC	EA	EA
210 °C	PA	PB	PC	EA

Figure 4 shows the EXCO macrographs in detail after immersion for 48 h. When the ending aging temperature is 150 and 170 °C, as shown in Fig. 4(a) and (b), notable layering and penetration to a considerable depth into the specimens can be seen for both the specimens and their corrosion ratings are ranked as EC. With the further increase of the ending aging temperature, the EXCO susceptibility slightly decreases and the corresponding corrosion depth becomes shallow (shown in Fig. 4(c)). When the ending aging temperature is not lower than 190 °C, only superficial exfoliation can be found on the surface (shown in Fig. 4(d)-(f)).

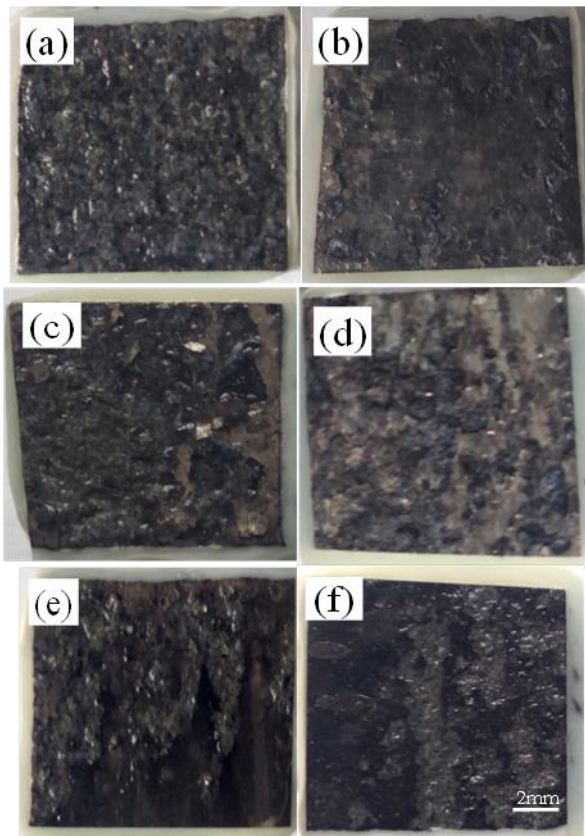


Figure 4 Surface morphologies of 7056 Al alloys after immersion in the EXCO solution for 48 h: (a) 150 °C; (b) 170 °C; (c) 180 °C; (d) 190 °C; (e) 200 °C; (f) 210 °C.

Figure 5 shows the TEM bright-field micrographs of the microstructure of 7056 alloys after non-isothermal aging at heating rates of 20, 40 and 60 °C/h. The corresponding ending aging temperature is 190 °C. At the heating rate of 20 °C/h (shown in Fig. 5(a)), the strong diffraction fringes corresponding to η precipitates in grain interiors are indexed at $1/3\{220\}$ and $2/3\{220\}$ positions along $\langle 110 \rangle_{Al}$ axes and its size is about 30 nm. When the heating rate continuously increases, the size of grain precipitates becomes smaller and the intensity of the corresponding diffraction fringes is weaker, which means the decrease of the number of η precipitates. As shown in Fig. 5(e), the size of the grain precipitates is only around 10 nm and its shape is mainly elliptical when the heating rate is 60 °C/h. Only weak diffraction spots corresponding to η precipitates occur at the position of

$2/3\{220\}$ along $\langle 110 \rangle_{Al}$ axes, indicating the number of η precipitates is very few. Otherwise, the TEM micrographs focused on grain boundaries of 7056 alloys after non-isothermal aging at heating rates of 20, 40 and 60 °C/h are presented in Fig.5(b), (d) and (f). It can be found that discontinuous and coarse grain-boundary precipitates all occur for various heating rates when the ending aging temperature is 190 °C, and precipitates free zone (PFZ) is also very evident. With decreasing the heating rate, the size of grain-boundary precipitates becomes larger and the width of PFZ further increases (shown in Fig. 5(b) and (d)).

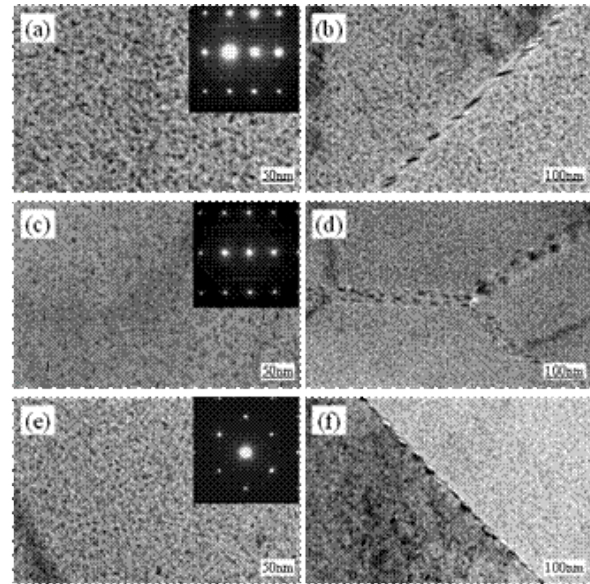


Figure 5 TEM images of the precipitates in grain interiors and grain boundaries for 7056 Al alloys after various heating aging rates: (a) (b) 20°C/h; (c) (d) 40°C/h; (e) (f) 60°C/h.

Figure 6 shows the TEM bright-field images of the non-isothermal aged 7056 Al alloys at a heating rate of 40 °C/h. It can be observed that the high density precipitates are homogeneously distributed in grain interiors and exhibit spherical, elliptical and needle contrast during non-isothermal aging, similar to isothermal aging. However, the average size of the grain precipitates is smaller and its density is higher at the same aging temperature compared to isothermal aging. As shown in Fig. 6(a), coherent spherical GP (Guinier-Preston) zones and semi-coherent η phase with a size of several nanometer are distributed in grain interiors when the ending aging temperature is 150 °C. With the increase of the ending aging temperature, the precipitates become coarser, as shown in Fig. 6(b) and (c). The density of the needle precipitates and the spacing between them both increase when the ending aging temperature is not lower than 190 °C. Therefore, when the ending aging temperature is set to 200 °C, the average size of the precipitates is found to be about 10 nm (shown in Fig. 6(e)). Further increasing the ending aging temperature to 210 °C, its average size is up to 20 nm (shown in Fig. 6(f)).

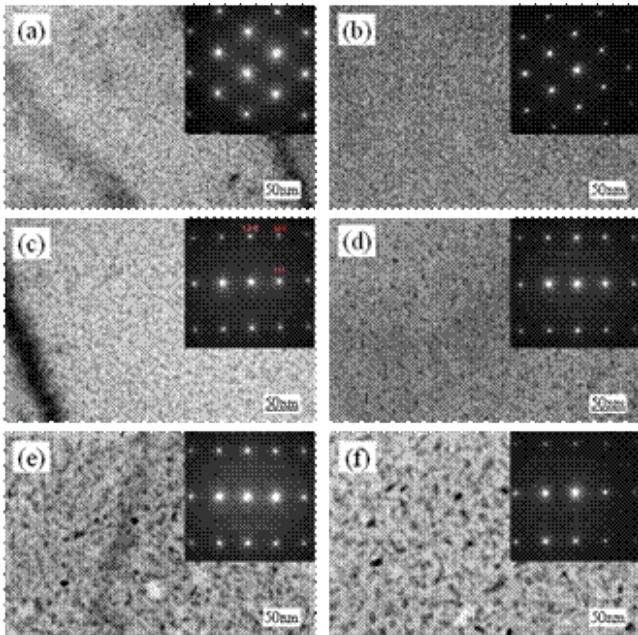


Figure 6 TEM bright-field images of the grain precipitates of 7056 Al alloy aged at various ending temperatures at a heating rate of 40 °C/h: (a) 150 °C; (b) 170 °C; (c) 180 °C; (d) 190 °C; (e) 200 °C; (f) 210 °C.

The TEM images focused on grain boundaries of the non-isothermal aged 7056 Al alloys at a heating rate of 40 °C/h are shown in Fig. 7. Continuous rod-like precipitates occur on grain boundaries and the width of grain boundaries is relatively narrow (between about 10 and 20 nm) when the ending aging temperature is 150 °C (shown in Fig. 7(a)). The spacing of the grain-boundary precipitates increases with increasing the ending aging temperature. When the ending aging temperature is set to be 200 °C, it can be seen from Fig. 7(e) that the width of grain boundaries slightly increases and PFZ corresponding to white area occurs along grain boundaries. When the ending aging temperature further increase to 210 °C (shown in Fig. 7(f)), discontinuous precipitates are found on grain boundaries, and PFZ surrounds coarse precipitates on grain boundaries. It can be found that the formation of PFZ is very difficult during the linear heating process compared with non-isothermal aging process. It is generally believed that the width of PFZs varies significantly with solution treatment temperature, quenching rate, aging treatment and deformation process. The PFZs are obvious since the precipitates slowly grow with a slow cooling rate during the non-isothermal aging. In this work, the width of PFZs is relatively narrow due to an insufficient content of solutes resulting from rapid heating of non-isothermal aging.

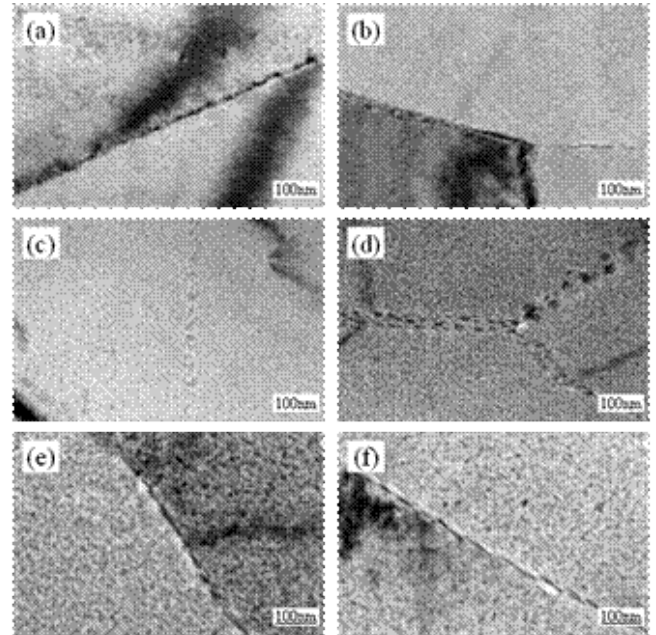


Figure 7 TEM bright-field images of the precipitates on grain boundaries of 7056 Al alloy aged at various ending temperatures at a heating rate of 40 °C/h: (a) 150 °C; (b) 170 °C; (c) 180 °C; (d) 190 °C; (e) 200 °C; (f) 210 °C.

In the present work, the above results show that the heating rate and ending aging temperature obviously affect the microstructure, mechanical properties and corrosion resistance of the non-isothermal aged 7056 Al alloys. The strengthening mechanism of Al-Zn-Mg-Cu alloys is mainly based on precipitation strengthening. The dimension, spacing and quantity of the grain precipitates basically decide the strength of aluminum alloys. It is generally accepted that fine and homogeneously distributed precipitates with high density can enhance the hardness and strength of aluminum alloys. Compared with isothermal aging, the non-isothermal aging process can provide a higher density of the fine metastable precipitates distributed homogeneously in Al matrix at the same aging temperature due to rapid variation of aging temperature. Therefore, the hardness and tensile strength of the non-isothermal aged 7056 Al alloys are relatively higher than those in peak-aged temper. When the ending aging temperature is the same, the higher heating rate during non-isothermal aging process means the shorter aging time, as shown in Fig. 5(a), (c) and (e), the coarsening of precipitates becomes weaker. This suggests that the hardness and strength of the 7056 Al alloy can be enhanced by increasing the heating rate. At the same heating rate, the size and quantity of the precipitates in grain interiors obviously increase with the increase of the ending aging temperature from 150 to 190 °C, as shown in Fig. 6(a)-(e). The rapid precipitation at the initial stage of non-isothermal aging process leads to the quick hardening, and the coarsening of the precipitates at the temperature range from 190 to 210 °C, which contributes to the consequent decrease in the hardness and strength.

It is well known that the SCC resistance can be enhanced with the increase of electrical conductivity in Al-Zn-Mg-Cu alloys. Therefore, the above results on electrical conductivity suggest that the slower heating rate and the higher ending aging temperature during non-isothermal aging can improve SCC resistance of 7056 Al alloys. As shown in in Fig. 5 and Fig. 7, the formation of discontinuous and coarse grain-boundary precipitates during non-isothermal aging are believed to be responsible for the enhancement of SCC resistance of 7056 Al alloys. As for IGC behaviors of 7056 Al alloys subjected to non-isothermal aging, it is well accepted that discontinuous distribution of grain-boundary precipitates or widening of the PFZ may be helpful to improve the SCC and IGC resistance of the alloys [21]. During non-isothermal aging, with increasing the ending aging temperature, the grain-boundary precipitates coarsen and gradually become discontinuously distributed on grain boundaries, accompanied by the formation and widening of the PFZ, which are beneficial to the enhancement of IGC resistance of 7056 Al alloys. It has been reported that the corrosion potentials of PFZ and Al matrix are generally positive compared with that of the grain-boundary precipitates in Al-Zn-Mg-Cu alloy [21]. Therefore, the potential differences among the matrix, grain-boundary precipitates and PFZ leads to anodic dissolution of the grain-boundary precipitates and IGC. Meanwhile, EXCO is developed from IGC, and widely regarded as a special form of IGC [22]. With the increase of the ending aging temperature, the Cu content of grain-boundary precipitates distinctly increases due to the increase of the diffusion rate of Cu atom. The composition variation of the grain-boundary precipitates can reduce the potential difference among Al matrix, grain-boundary precipitates and PFZ [23, 24]. This leads to the decrease of the dissolution rate of the corrosion. As a result, IGC and EXCO resistance of 7056 Al alloy subjected to non-isothermal aging can be obviously enhanced by increasing the ending aging temperature.

IV. CONCLUSION

In summary, The effects of the heating rate and ending aging temperature on microstructure, mechanical properties and corrosion behaviors of a high Zn-containing 7056 Al alloy during non-isothermal aging process have been investigated. Excellent mechanical properties and satisfactory corrosion resistance can be obtained by non-isothermal aging process. Under the heating aging conditions the higher heating rate can enhance the electrical conductivity of 7056 Al alloy but induce the decrease of the hardness. During non-isothermal aging the hardness and strength of 7056 Al alloy are up to the maximum value of 210 HV and 700 MPa, respectively, when the ending aging temperature is between 180 °C and 190 °C. Further, the hardness decreases with the ending aging temperature over 200 °C. The variations of mechanical properties and corrosion resistance during non-isothermal aging are closely related with

the size, quantity and distribution of the precipitates in grain interiors and grain boundaries.

ACKNOWLEDGMENT

The work was primarily financial supported by the National Key R&D Program of China (Grant No. SQ2017YFE030085), State Key Laboratory for Powder Metallurgy and Open sharing Fund for the Large-scale Instruments and Equipments for Central South University.

REFERENCES

- [1] A. Heinz, A. Haszler, C. Keidel, S. Moldenhauer, W. S. Miller, *Mater Sci Eng A*. 2000, 280(1), 102-107.
- [2] T. Dursun, C. Soutis, *Mater. Des.* 2014, 56, 862–871.
- [3] J. C. Williams, E. A. Starke, *Acta Mater.* 2003, 51, 5775-5799.
- [4] R. Casati, M. Coduri, M. Ricco, A. Rizzi, M. Vedani, *J Alloys Compd.* 2019, 801, 243-253.
- [5] H. A. Elhadari, H. A. Patel, D. L. Chen, W. Kasprzak, *Mater Sci Eng A*. 2011, 528, 8128-8138.
- [6] Y. L. Deng, Y. Y. Zhang, L. Wan, X. M. Zhang, *Mater Sci Eng A*. 2012, 554, 33–40.
- [7] S. Y. Chen, J. Y. Li, G. Y. Hu, K. H. Chen, L. P. Huang, *J Alloys Compd.* 2018, 757, 259-264.
- [8] B. Liu, Q. Lei, L. Q. Xie, M. P. Wang, Z. Li, *Mater Des.* 2016, 96, 217–233.
- [9] M. Ebrahimi, M. H. Shaeri, R. Naseri, C. Gode, *Mater Sci Eng A*. 2018, 731, 569-576.
- [10] J. Adrien, E. Maire, R. Estevez, J. C. Ehrstrom, T. Warner, *Acta Mater.* 2004, 52, 1653–1661.
- [11] S. Y. Chen, K. H. Chen, G. S. Peng, L. Jia, P. X. Dong, *Mater Des.* 2012, 35, 93–98.
- [12] T. Marlaud, A. Deschamps, F. Bley, W. Lefebvre, B. Baroux, *Acta Mater.* 2010, 58, 4814-4826.
- [13] J. T. Staley. Durham US Patent, 0237113A1, 2007.
- [14] J. T. Jiang, W. Q. Xiao, L. Yang, W. Z. Shao, S. J. Yuan, L. Zhen, *Mater Sci Eng A*. 2014, 605, 167-175.
- [15] X. Y. Peng, Q. Guo, X. P. Liang, Y. Deng, Y. Gu, G. F. Xu, Z. M. Yin, *Mater Sci Eng A*. 2017, 688, 146-154.
- [16] Y. Liu, D. M. Jiang, B. Q. Li, W. S. Yang, J. Hu, *Mater Des.* 2014, 57, 79-86.
- [17] J. T. Jiang, W. Q. Xiao, L. Yang, W. Z. Shao, S. J. Yuan, L. Zhen, *J Mater Process Technol.* 2016, 227, 110-116.
- [18] D. M. Jiang, Y. Liu, S. Liang, W. L. Xie, *J Alloys Compd.* 2016, 681, 57-65.
- [19] X. Y. Peng, Y. Li, X. P. Liang, Q. Guo, G. F. Xu, Y. Y. Peng, Z. M. Yin, *J Alloys Compd.* 2018, 735, 964-974.
- [20] T. C. Tsai, T. H. Chuang, *Mater Sci Eng A*. 1997, 225, 135-144.
- [21] S. D. Liu, B. Chen, C. B. Li, Y. Dai, Y. L. Deng, X. M. Zhang, *Corros Sci.* 2015, 91, 203-212.
- [22] X. H. Lu, X. L. Han, Z. W. Du, G. J. Wang, L. Y. Lu, J. Q. Lei, T. T. Zhou. *Mater Char.* 2018, 135, 167-174.
- [23] L. P. Huang, K. H. Chen, S. Li, *Mater Sci Eng B*. 2012, 177, 862-868.
- [24] Y. R. Liu, Q. L. Pan, H. Li, Z. Q. Huang, J. Ye, M. J. Li, *J Alloys Compd.* 2019, 792, 32-45.